Analysis Of Mutual Inductance Between Transmitter And Receiver Coils In Wireless Power Transfer System Of Electric Vehicle

Junlong ZHENG[1,2], *Chaiyan JETTANASEN*[1]

[1]School of Engineering, King Mongkut's Institute of Technology Ladkrabang. Bangkok 10520, Thailand;
[2] Guangxi Electrical Polytechnic Institute. Nanning, Guangxi, China;

long8889@126.com, chaiyan.je@kmitl.ac.th

DOI: 10.15598/aeee.v21i3.4991

Article history: Received Dec 24, 2022; Revised Mar 20, 2023; Accepted Sep 08, 2023; Published Sep 30, 2023.

Abstract. *In the electric vehicle wireless power transfer (WPT) system, the mutual inductance (M) between the transmitting and receiving coils is an important factor influencing overall system efficiency. The M is affected by various factors such as the physical structure of the coils diagram, the distance and relative position between the transmitting and receiving coils, and so on. Our work here has two outstanding contributions. First, the detailed mathematical model of the M was developed. Second, the three-dimensional spatial distribution diagram of the M was drawn using Python software, the maximum value of the M and its corresponding position coordinates were calculated. Then, the theoretical analysis of the M distribution was proven correct through experiments. The theoretical analysis and experimental verification of the M distribution provided a theoretical reference for the positioning requirements between the transmitting and receiving coils.in the electric vehicle WPT system.*

Keywords

Electric vehicle, Wireless power transfer; Magnetic field, Mutual inductance.

1. Introduction

The wireless charging technology for electric vehicles transmits electric energy in the form of high-frequency alternating magnetic energy to the electric energy pickup mechanism at the receiving end via the electric energy transmitting coil, and then supplies power to the on-board energy storage equipment; wherein the power transmitting coil is buried under the ground or installed on the ground; and the electric energy pickup mechanism at the receiving end is installed on the automobile chassis.

Magnetic coupling resonance wireless power transmission system (abbreviated as MCR-WPT) is the most prevalent type of electric vehicle wireless charging technology. The overall system composition is depicted in Fig.1-1. The system is made up of a rectifier filter circuit. ①, high-frequency inverter circuit ②, drive circuit, sampling circuit, resonant capacitors C1 C2, transmitting coil L1, receiving coil L2, high-frequency rectifier circuit ④ and load circuit ⑤. Among these, the 220V mains power input rectifier filter circuit ① generates direct current Ui Ii, which is then delivered to the high-frequency inverter circuit ② to generate a specified frequency of AC power. The frequency of this alternating current power can be regulated by the driving circuit; this AC power is given to the resonant circuit module ③, allowing for wireless transfer of electrical energy. Module ③ is made up of two LC resonant circuits, L1 and L2, as well as corresponding resonant capacitors C1 and C2 [1].

The MCR-WPT's energy transmission performance is largely dependent on the position connection between the emitter and receiver coils, according to its working principle [3]. The primary focus of MCR-WPT system research, as well as the major factor that directly effects MCR-WPT system use and promotion, is how to ensure the successful transmission of electric energy in MCR-WPT system.

For the MCR-WPT system research, Lionel Pichon [2] made a detailed analysis of the magnetic induction strength. Rui Feng et al [3] detailed analyzed of magnetic field distribution. Yang Yang et al [4], optimized the shape and structure of transmitting and receiving coils. Kafeel Ahmed Kalwar, et al [5], proposed a new coil design qad D quadrature. Sangwook Park [6] maded electromagnetic exposure assessment and analyzed the impact of different exposure scenes on human body. Haris Gulzar, et al [7], made a comprehensive electromagnetic design for MCR-WPT, and experiments verified that MCR-WPT can transmit power wirelessly with an efficiency of more than 85%. Rupesh Kumar Jha et al [8] analyzed the unit resonant topology used for WPT, and the performance of the topology is comprehensively evaluated and compared. Ihssen Jabri et al [9] analyzed the influence of transverse misalignment and separation distance between primary and secondary coils. Metaheuristic algorithm and genetic algorithm were used to optimize the design of primary and secondary coils. Despite the fact that researchers and specialists from all over the world have conducted extensive research on MCR-WPT, we discovered no precise analysis of the M between the transmitting and receiving coils, nor a particularly specific mathematical model. As a result, it is vital to study the M.

2. Main factors affecting MCR-WPT efficiency

In Fig. 1, the MCR-WPT system is shown to be operating in a fully resonant state. According to technical standards, only a very small amount of the overall power of the MCR-WPT system is accounted for by the loss power of the high-frequency inverter circuit and the loss power of the high-frequency rectifier filter circuit. The efficiency of the MCR-WPT system is given as formula (1) [1] if the calculation is not exceedingly precise and negligibly. The term "efficiency η" used in the full text refers to the overall effectiveness η of the MCR-WPT system.

$$\eta = \frac{P_o}{P_i} = \frac{U_O I_O}{U_i I_i} \approx \frac{\omega_d^2 M^2 R_L}{(R_2 + R_L)(\omega_d^2 M^2 + R_1 R_L + R_1 R_2)}, \quad (1)$$

where Po is the total output power of MCR-WPT system, Pi is the total input power of MCR-WPT system, Ui, Ii, Uo, Io as shown in Fig. 1, respectively represent the input and output voltage and current of the entire MCR-WPT system, M the mutual inductance between transmitting coil and receiving coil, RL equivalent load at the output end of the resonance unit at the receiving end, R1 represents the series equivalent resistance of the equivalent resistance of the transmitting coil and the AC equivalent resistance of the compensation capacitor, R2 represents the series equivalent resistance of the equivalent resistance of the receiving coil and the AC equivalent resistance of the compensation capacitor, ωd is the driving angular frequency of the high-frequency inverter when the system operates in the fully resonant state, η efficiency of the whole MCR-WPT system.

To better understand the relationship between η and M, the expression is translated into the formula (2):

$$\frac{1}{\eta} = 1 + \frac{R_2}{R_L} + \frac{(R_2 + R_L)(R_1 R_L + R_1 R_2)}{\omega_d^2 M^2 R_L}, \quad (2)$$

It can be seen from formula (2) that the η has a positive relationship with the M and ωd, which means that as M or ω_d increases, so the η does.

In the MCR-WPT system, the η needs to be increased in order to increase the total output power Pout, once the total input power Pin is established; We can think about enhancing the M and the ωd; The ωd, on the other hand, is determined by the resonance unit's natural frequency and is directly related to the parameters of the coil inductance coefficient, resonance capacitance, and other electrical components of the resonance unit. The ωd and the resonance frequency are determined when these electrical parameters are determined. Therefore, only the M is left to be the focus of efforts to increase the resonance unit's efficiency and, consequently, increase the MCR-WPT system's overall output power Pout [11, 12].

As can be seen, the M is one of the key factors affecting the η. The M can be expressed using formula (3) from [15] according to its definition

$$M = \frac{\Phi}{I}, \quad (3)$$

where, I is the current passing through the transmitting coil, Φ is the magnetic flux generated by the transmitting coil surrounded by the receiving coil.

Where, the magnetic flux Φ is affected by the relative position between the two coils, coil shape, coil winding cycles and other factors, and then affects the M. To improve the transmission efficiency of the MCR-WTP system, it is necessary to improve the M. Therefore, it is necessary to study the magnetic flux Φ in the relative position between the two coils.

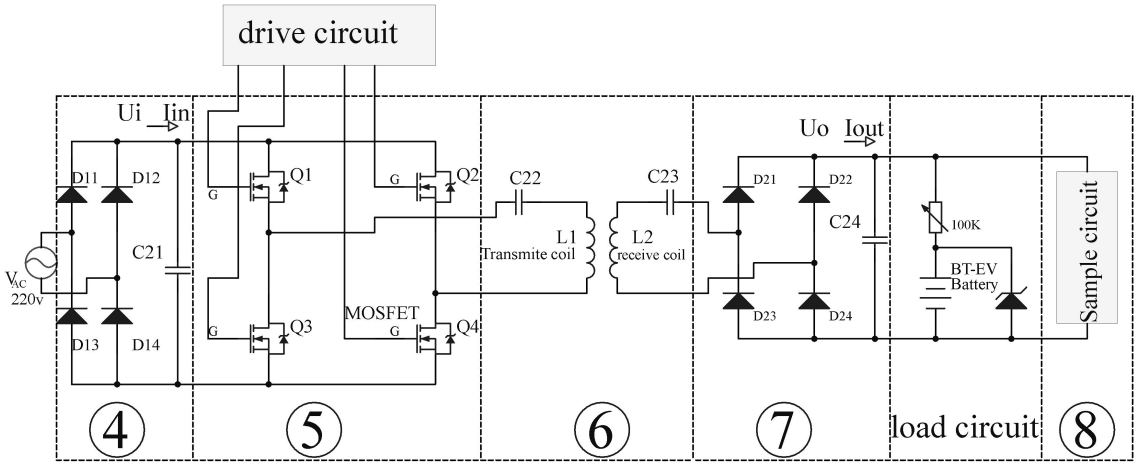

Fig. 1: MCR-WPT System Component Circuit Diagram [1].

3. Math model of magnetic field for the L1 in MCR-WPT system

According to Biot Savart Law, through geometric analysis and mathematical operation, as shown in Fig. 2, the component Bz_rectangle in the Z direction of the magnetic induction intensity generated at any point P(x, y, z) in the space of the electrified rectangular coil with length L and width W can be obtained as formula (4) [13], where μ_0 is the permeability in vacuum, $\mu_0 = 4\pi \times 10^{-7}$, unit: T.m/A, the permeability in the air is close to the vacuum permeability, and the vacuum permeability can often be directly used in the calculation [10], I is the current intensity passing through the coil, unit A, L.W is the length and width of the coil, unit m, Bz_rectangle is the magnetic induction intensity of point P in the Z direction in the magnetic field generated by the rectangular coil, unit T.

In this paper, the electric vehicle wireless charging system studied is the MCR-WPT system. The magnetic coupling resonance mechanism of the system is mainly composed of the transmitting coil and receiving coil [14].

Fig. 3 depicts the transmission coil built in reference [16] in this paper. The shape of the coil is approximately rectangular, and it is wound by double wires 8 times. The length and width of the coil are 650 × 500mm; Inner space size is about 350 × 200mm, with an average width of about 37.5mm (0.0375m) per week. For the convenience of calculation, first calculate according to the single wire, and then multiply the calculation result by 2 to obtain the total magnetic induction intensity generated by the transmitting coil at any point in space.

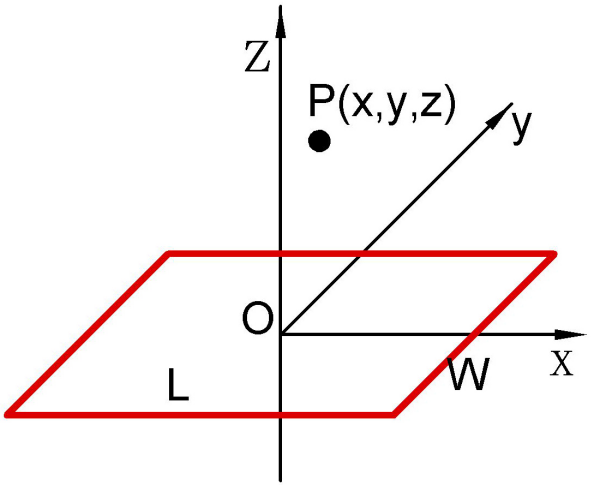

Fig. 2: Schematic diagram of any point P in the magnetic field space of the energized rectangular coil.

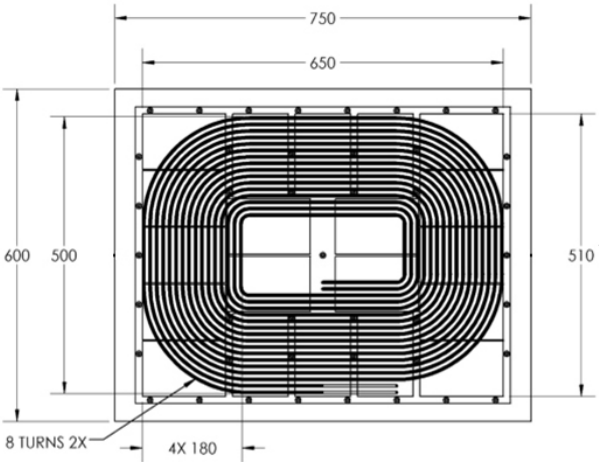

Fig. 3: Planar graph of transmitting coil [16].

$$B_{z\_rectangle} = \frac{\mu_0 I(W-y)}{4\pi\left[z^2+(W-y)^2\right]}\left(\frac{L-x}{\sqrt{(x-L)^2+(y-L)^2+z^2}}+\frac{L+x}{\sqrt{(x+L)^2+(y-L)^2+z^2}}\right)$$
$$+\frac{\mu_0 I(L+x)}{\pi\left[z^2+(L+x)^2\right]}\left(\frac{W-y}{\sqrt{(x+L)^2+(y-W)^2+z^2}}+\frac{W+y}{\sqrt{(x+L)^2+(y+W)^2+z^2}}\right)$$
$$+\frac{\mu_0 I(W+y)}{\pi\left[z^2+(W+y)^2\right]}\left(\frac{L+x}{\sqrt{(x+L)^2+(y+W)^2+z^2}}\frac{L-x}{\sqrt{(x-L)^2+(y+W)^2+z^2}}\right)$$
$$+\frac{\mu_0 I(L-x)}{\pi\left[z^2+(L-x)^2\right]}\left(\frac{W+y}{\sqrt{(x-L)^2+(y+W)^2+z^2}}+\frac{W-y}{\sqrt{(x-L)^2+(y-W)^2+z^2}}\right), \quad (4)$$

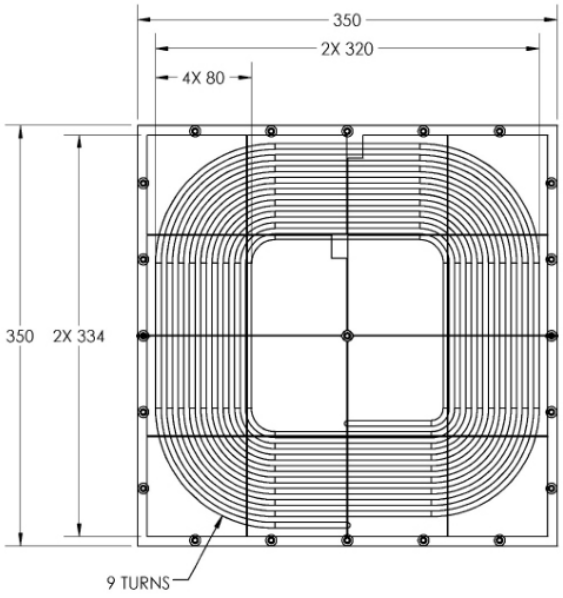

Fig. 4: Planar graph of receiving coil [16].

According to formula (4) calculation method of magnetic induction strength of a rectangular coil. The calculation formula of the magnetic induction intensity component Bz generated in space by the MCR-WPT transmission coil wound 8 times in the above figure can be obtained as formula (5), where, L, W is the length and width of the transmitting coil, unit m. In this paper, 0.65m and 0.50m are taken respectively, g is the average line width of each cycle of the coil, taken as 0.0375m in this paper, i is the cumulative ordinal number; Initial value i = 0, i=i+1<=7, Bz is the magnetic induction intensity of point P in the Z direction in the magnetic field generated by the transmitting coil, unit T.

Next, the magnitude of the effective magnetic flux of the receiving coil in the magnetic field generated by the transmitting coil is calculated. The receiving coil designed in this paper is obtained from reference [16], as shown in Fig. 4.

The coil shape is almost square, with the length and breadth of 350×350mm, and the effective magnetic flux surrounding by the receiving coil's outermost cycle can be determined using the double integrating formula (5).

Because the area enclosed by the coil in each cycle is reduced equidistantly from the outside to the inside, the integration area of each cycle is reduced in turn to perform integration calculation, and then accumulated, so that the effective magnetic flux that contains all of the receiving coil's winding a few cycles, can be accurately calculated.

After obtaining the effective magnetic flux, according to formula (3), the M, which is defined by the magnetic flux Φ enclosed by the receiving coil, divided by the current I flowing through the transmitting coil. Combined with the above calculation of magnetic flux, the expression of the M can be obtained as formula (10).

Where, the M is derived by combining formula (3) and formula (5)

$$M = \frac{\Phi}{I} = \frac{2}{I} \times \sum_{j=0}^{8} \iint_{D_j} B_z dx dy, \quad (6)$$

Φ is the magnetic flux generated by the transmitting coil surrounded by the receiving coil. Because the receiving coil is wound for nine cycles, it is cumulative, and because it is wound for two wires, it is multiplied by 2, Dj is the integral closed region. The receiving coil is shown in the Fig. 4. Since the area surrounded by the coil is reduced by equal distance from the outside to the inside, the integral area of each cycle is reduced in turn to calculate the integral, and then accumulated, the effective magnetic flux contained in all the coils wound for 9 cycles of the receiving coil can be accurately calculated.

$$D_J = x_j \cdot y_j, \quad (7)$$

$$x_0 - \frac{k}{2} + jr \leqslant x_j \leqslant x_0 + \frac{k}{2} - jr, \quad (8)$$

$$y_0 - \frac{h}{2} + jr \leqslant y_j \leqslant y_0 + \frac{h}{2} - jr, \quad (9)$$

$$
\begin{aligned}
B_z = {} & 2 \times \sum_{i=0}^{7} \frac{\mu_0 I((W-gi)-y)}{4\pi\left[z^2+((W-gi)-y)^2\right]} \\
& \times \left(\frac{(L-gi)-x}{\sqrt{(x-(L-gi))^2+(y-(W-gi))^2+z^2}} + \frac{L-gi+x}{\sqrt{(x+(L-gi))^2+(y-(W-gi))^2+z^2}} \right) \\
& + \frac{\mu_0 I(L-gi+x)}{\pi\left[z^2+(L-gi+x)^2\right]} \left(\frac{W-gi-y}{\sqrt{(x+L-gi)^2+(y-(W-gi))^2+z^2}} + \frac{W-gi+y}{\sqrt{(x+L-gi)^2+(y+W-gi)^2+z^2}} \right) \\
& + \frac{\mu_0 I(W-gi+y)}{\pi\left[z^2+(W-gi+y)^2\right]} \left(\frac{L-gi+x}{\sqrt{(x+L-gi)^2+(y+W-gi)^2+z^2}} \frac{L-gi-x}{\sqrt{(x-(L-gi))^2+(y+W-gi)^2+z^2}} \right) \\
& + \frac{\mu_0 I(L-gi-x)}{\pi\left[z^2+(L-gi-x)^2\right]} \left(\frac{W-gi+y}{\sqrt{(x-(L-gi))^2+(y+W-gi)^2+z^2}} + \frac{W-gi-y}{\sqrt{(x-(L-gi))^2+(y-(W-gi))^2+z^2}} \right),
\end{aligned}
\tag{5}
$$

where r is the average interval width of each turn of the receiving coil, which is taken at 0.009m in this paper. i. j is the cumulative ordinal number, initial value i=0, step=1, i<=7, j<=8, k. h is the length and width of the receiving coil (m), which is taken as 0.35m and 0.35m respectively in this paper. (x0, y0) is a specific point in the XY plane from the height of the Z value of the transmitting coil. This point is the position where the center of the receiving coil is placed.

According to the preceding study, (x0, y0) is the coordinate of the receiving-coil center point, and its value range is x0 ∈ [-0.397, +0.397], y0 ∈ [-0.368, +0.368], and the unit is meter (m).

When (x0, y0) is appropriate, the M reaches its maximum value. At this time, (x0, y0) is the positioning point to be found by the receiving-coil center.

4. Calculation of the M

From formula (10), it can be expected that when the receiving coil's center is positioned at any point (x0, y0, Z), the calculation of M is quite complex and must be done on the computer using the program.

The pseudo code of the program is as follows:

```
The pseudocode for calculating the M:
Begin
Scientific computing module
Define the calculation range, variables
and parameters L,W,pai,u0,d
Define function F(x, y)
Define function FBz(x, y):
for i in range(0,8):
Bz = Bz + F(x, y)
L = L - 0.0375
W = W - 0.0375
return Bz
end for
Define integral function INF(x0,y0)
k=0.35, h=0.35, r=0.009
# Length, width and step of receiving
coil
for j in range(0,9):
# Superimpose the magnetic flux
surrounded by each turn of receiving
coil
xDlimit=x0-l/2+jr, xUplimit=x0+l/2-jr
yDlimit=y0-h/2+jr, yUplimit=y0+h/2-jr
Fi=Fi+integrate.nquad(FBz
(x,y), [[xDlimit, xUplimit],
[yDlimit,yUplimit]])
Return Fi
end for
Define the value range of x0 and y0:
x0 ∈ [-0.397, +0.397], y0 ∈ [- 0.368,
+0.368]
for p in range(0,100):
for q in range(0,100):
Fi = INF (x0[p,q],y0[p,q])
# Loop call INF function for integral
operation
Fi_list.append(Fi)
end for
Fi_array=array(Fi_list)
Plot(x0,y0,Fi_array)
end
```

In this paper, Python software is used to write an arithmetic program, set the receiving-coil center point (x0, y0) on the XY plane 20cm above the transmitting-coil, assign 900 coordinate points evenly distributed in the definition domain to (x0, y0), calculate the M of the two coils, and draw these values into the distribution diagram as Fig. 5 and Fig. 6.

$$
\begin{aligned}
M = 2 \times \sum_{j=0}^{8} \iint_{D_j} \sum_{i=0}^{7} & \frac{\mu_0((W-gi)-y)}{4\pi\left[z^2+((W-gi)-y)^2\right]} \\
\times & \left(\frac{(L-gi)-x}{\sqrt{(x-(L-gi))^2+(y-(W-gi))^2+z^2}} + \frac{L-gi+x}{\sqrt{(x+(L-gi))^2+(y-(W-gi))^2+z^2}} \right) \\
+ & \frac{\mu_0(L-gi+x)}{\pi\left[z^2+(L-gi+x)^2\right]} \left(\frac{W-gi-y}{\sqrt{(x+L-gi)^2+(y-(W-gi))^2+z^2}} + \frac{W-gi+y}{\sqrt{(x+L-gi)^2+(y+W-gi)^2+z^2}} \right) \\
+ & \frac{\mu_0(W-gi+y)}{\pi\left[z^2+(W-gi+y)^2\right]} \left(\frac{L-gi+x}{\sqrt{(x+L-gi)^2+(y+W-gi)^2+z^2}} + \frac{L-gi-x}{\sqrt{(x-(L-gi))^2+(y+W-gi)^2+z^2}} \right) \\
+ & \frac{\mu_0(L-gi-x)}{\pi\left[z^2+(L-gi-x)^2\right]} \left(\frac{W-gi+y}{\sqrt{(x-(L-gi))^2+(y+W-gi)^2+z^2}} + \frac{W-gi-y}{\sqrt{(x-(L-gi))^2+(y-(W-gi))^2+z^2}} \right) dxdy,
\end{aligned}
\tag{10}
$$

4-3.jpg

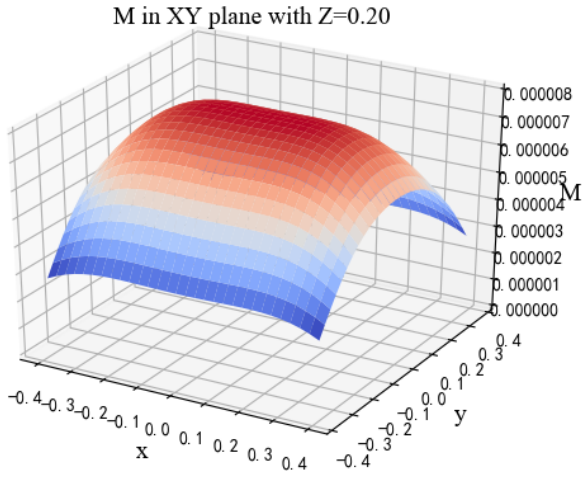

Fig. 5: M distribution map.

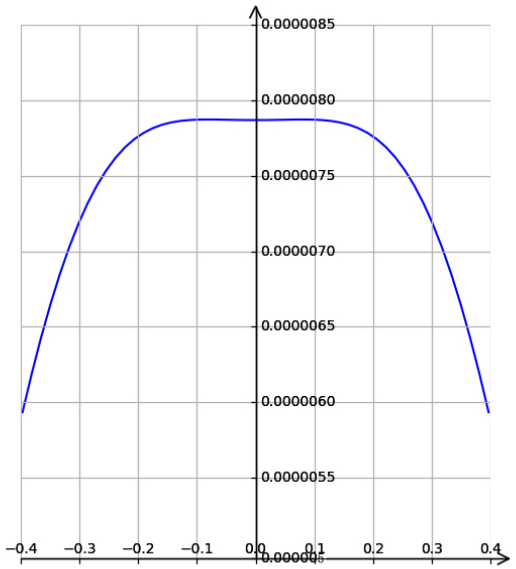

Fig. 7: Y=0,X-M graph.

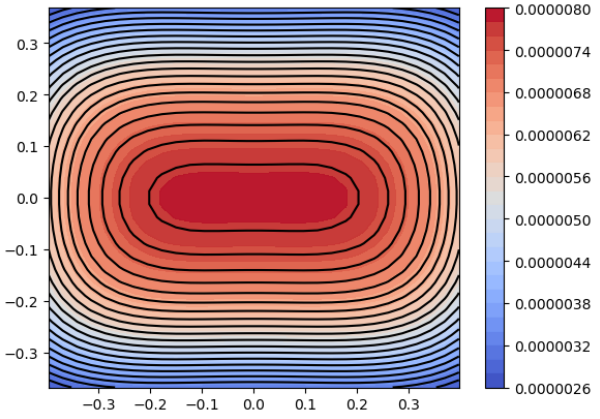

Fig. 6: M distribution contour map.

Fig. 5 and Fig. 6 show the continuous distribution of M in the area of x0∈[-0.397, +0.397], y0∈[-0.368, +0.368], z = 0.2m

Fig. 7 is the M-X distribution curve along the middle segment parallel to the X axis with y = 0 and z = 0.2;

Fig. 8 is the M-y distribution curve along the middle line segment parallel to the Y axis with x = 0 and z = 0.2;

From the Fig. 5 to Fig. 8 four figures, it can be seen that the M of the two coils is the largest when the receiving-coil is located near the right above the transmitting-coil, that is, when (x0, y0) is located near

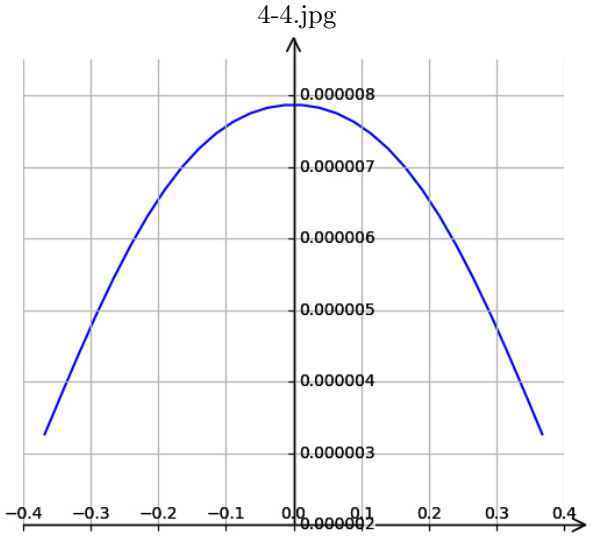

Fig. 8: X=0,Y-M graph.

the coordinate origin. Second, when the receiving-coil is located directly above the transmitting coil and is within the range of about 0.10m in the x-axis direction, M still obtains a value close to the maximum value. Third, when the receiving coil is located directly above the transmitting coil and translates along the y-axis direction, the value of M rapidly decreases. This is due to the influence of the rectangular structure of the transmission coil.

The maximum value of the M is obtained by using Python software to run the computer program.

$$\text{Mmax} = 7.87 \times 10^{-6}(H) \tag{11}$$

5. Construction of experimental platform

The L1 is positioned on the x-axis slide, as shown in Fig. 9, and the entire set of x-axis screw slides is fastened on two synchronously moving Y-axis slides. Using three sets of screw slides, a "H" type XY two axis motion unit is built in this way. In order to move the L1 in XY directions, the MCU (Microcontroller Unit) principally controls the SMD (Steppe Motor Driver), which drives the stepper motors in two directions. Fig. 10 depicts the general installation architecture of the MCR-WPT experimental platform.

Among them, the portion of WPT for electric vehicles is designed by reference [1]. Fig. 11 and Fig. 12 depict the physical layout of the entire MCR-WPT system. When constructing an experimental platform, the load circuit is replaced with a high-power electric water heater to make experimental operation easier. Theoretically, the experiment of wireless power transfer won't be affected by such a simplification of component substitution.

The next step is to calculate the resonant capacitance C1 C2. First, the L1 and L2 are measured three times by an inductance meter, and then the average is calculated. One of the measurements is shown in Fig. 13 and Fig. 14.

Three measurements of L1 produced results of 52.515μH, 52.576 μH, 52.462 μH, with an average of 52.518 μH.

Three measurements of L2 produced results of 25.672μH, 25.642μH, 25.728μH, with an average of 25.681μH.

Formula (12). [17]: can be used to determine the resonant capacitance after the coil's inductance has been determined:

$$C = \frac{1}{(2\pi f)^2 L} \tag{12}$$

where C is a resonant capacitor, f is the resonant frequency, taking 85kHz [17], L is the inductance of the coil.

The values obtained from the direct measurement of L1 and L2 are substituted, and it is discovered that C1 and C2 should be 66.8 and 136.5nf, respectively.

Working principle of the system: Combined with Fig. 1 and Fig 11, Fig 12, the ① is an adjustable DC voltage regulator, and the high frequency inverting circuit ② can get direct current from ① to convert direct current into high frequency alternating current, which is controlled by the frequency of pulse signal PWM (Pulse width modulation) of the grid drive circuit ⑦⑧. Then the alternating current is supplied to the resonance circuit formed by L1C1. L1 transmits energy to L2 in the form of alternating magnetic field. L2C2 also forms a resonance circuit, because we design L1C1 with the same inherent frequency as L2C2, adjust the frequency of PWM, thereby changing the frequency of alternating current supplied to L1C1; When the frequency of the alternating current equals the inherent frequency of the two LC components, they work in a resonant state. The magnetic field coupling resonance occurs between the L1 and L2, which generates a high frequency alternating magnetic field which radiates to the L2, thus generating an inductive current and realizing the wireless transmission of energy. L2C2 transmits the inductive current to the high frequency rectifier filter circuit ④ and obtains the direct current supply to the load circuit ⑤. The upper computer ⑨ is used to collect data through the sample circuit ⑥ and change the frequency of PWM.

Fig. 9, Fig. 10, Fig. 11 and Fig. 13 notes:

1. Active range for Transmit coi;

2. Y-axis positive direction limit position sensor;
3. X-axis negative direction limit position sensor;
4. Y-axis negative direction limit position sensor;
5. X-axis positive direction limit position sensor;
6. Y-axis screw rod one;
7. Y-axis screw rod two;
8. X-axis screw rod;
9. Transmitting-coil;
10. Y-axis sliding-table-one;
11. X-axis sliding table;
12. Y-axis sliding-table-two;
13. Active range for center point of receiving-coil;
14. receiving-coil;
15. Glass cover;
16. Parking space ground;

① Adjustable DC regulated power supply
② Full bridge inverter circuit module;
③. L1, L2, C1 and C2 together constitute module ③;
④ Full bridge rectifier filter circuit in output module;
⑤. Load resistance in the output module;
⑥ Output voltage and current sampling circuit;
⑦ gate drive circuit one;
⑧ gate drive circuit two;
⑨.Upper computer;

MCU. Microcontroller Unit;
Y-SM. Stepper motor in Y-axis;
X-SM. Stepper motor in X-axis;
Y-SMD. Stepper motor driver in Y-axis;
X-SMD. Stepper motor driver in X-axis;
L1. Transmitting-coil;
L2. receiving-coil;
DSP. Digital Signal Processing;
DC. 15V DC regulated power supply;
C1. Resonant capacitance at the transmitter;
C2. Resonant capacitance at the receiver;

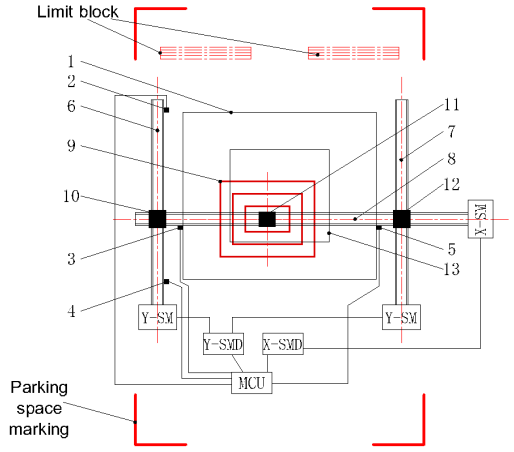

Fig. 9: Diagram of the MCR-WPT experimental platform.

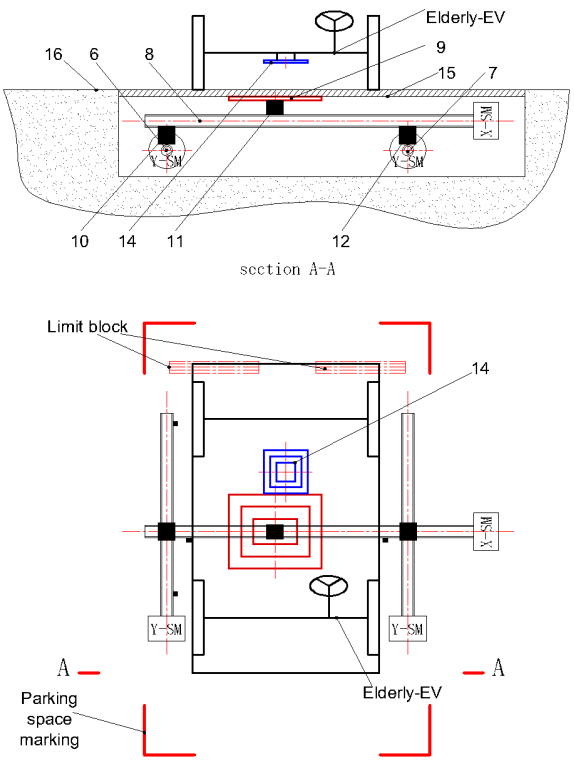

Fig. 10: Overall installation layout of the MCR-WPT experimental platform.

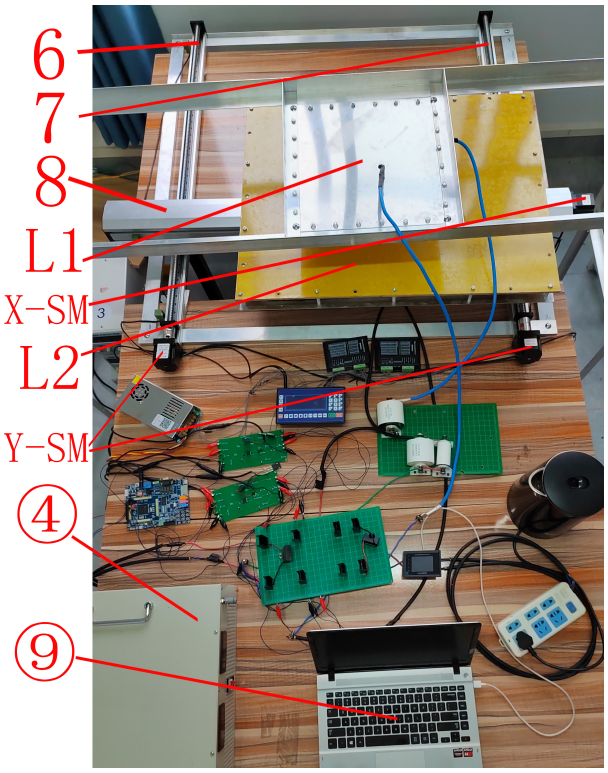

Fig. 11: Photos of the MCR-WPT experimental platform.

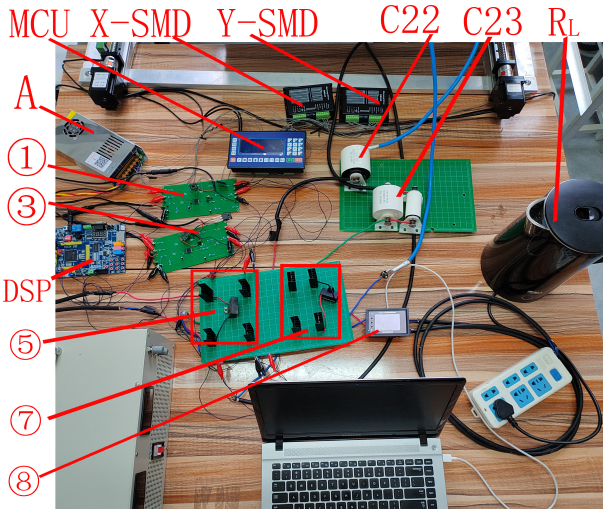

Fig. 12: Partial detail of the MCR-WPT experimental platform.

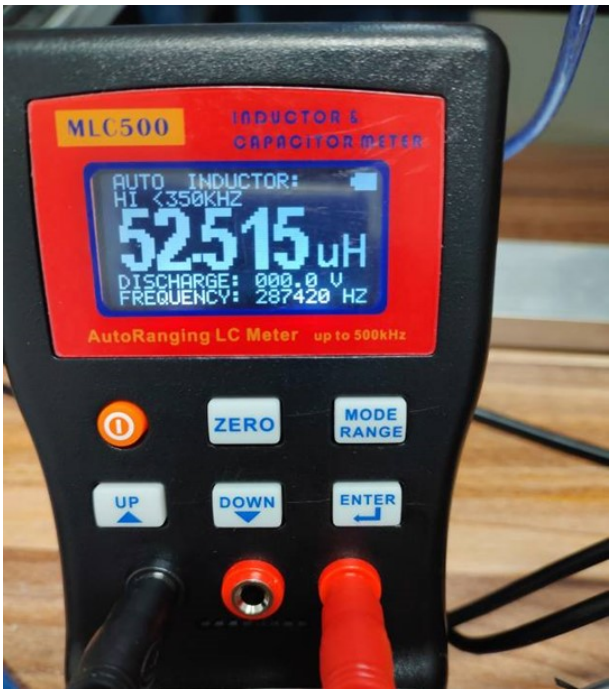

Fig. 13: L1 inductance measurement.

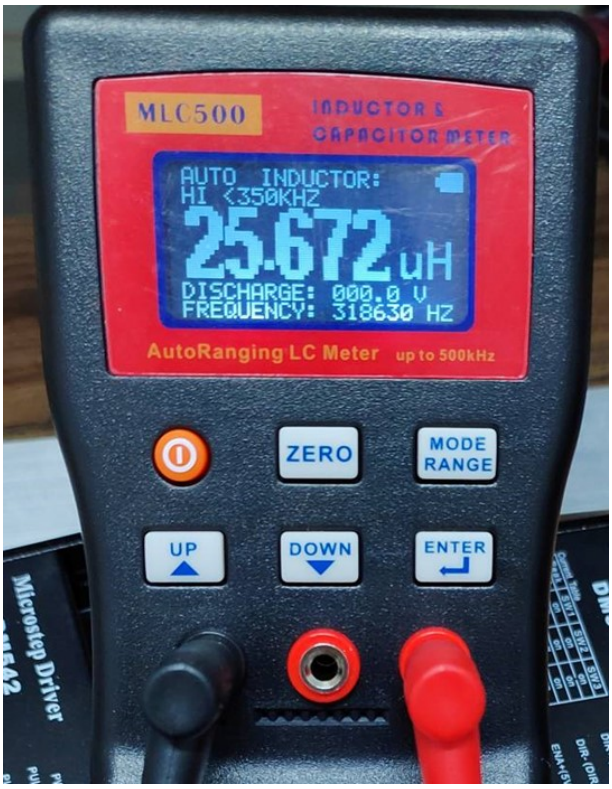

Fig. 14: L2 inductance measurement.

6. Analysis of experimental data

Experiment 1:Input DC voltage Ui=400V to MCR-WPT system, Distance D=20CM between transmitting-coil L1 and receiving-coil L2, System load resistance RL=70 Ω, Entered drive frequency f=80.0∼89.0KHz, the experimental data are shown in Table 1.

Except for MCR-WPT efficiency η, all of the data in Table 1 is directly recorded during the experiment. The η is derived using the formula (13):

$$\eta = \frac{P_o}{P_i} = \frac{U_o I_o}{U_i I_i} \tag{13}$$

where, η, Po, Pi, Uo, Io, Ui, Ii, are the same as the definition above.

By analysing the data in Table 1 and combining theoretical knowledge of MCR-WPT, it can be seen that the resonant frequency of MCR-WPT of this experimental platform is 85.3 kHz, and the corresponding maximum η is 80.41%.

Experiment 2: Carry out the M distribution experiment with drive frequency f=85.3khz, input voltage Ui=400v, distance D=20CM between transmitting coil L1 and receiving coil L2, system load resistance RL=70 Ω. By programming, the MCU can record in detail the 900 coordinate points evenly distributed in the defined interval [-0.4, +0.4], and the data about the input-output voltage and current values corresponding to the coordinate points during the experiment. The coordinate position takes the L1 center point as the coordinate origin. Table 2 is the arrangement of experimental data. There are 900 rows of data in total. Due to the space limitation, it is difficult to list all the 900 rows of data in Table 2. Only the first 8 lines and the last 12 lines of data near the maximum value of M are listed in this table.

Not all of them are listed due to the enormous amount of data. To evaluate the data more intuitively, all 900 lines of data are drawn into an intuitive and visual representation using Python software, as illustrated in Fig. 15 and Fig. 16.

Data in Table 2, except for the η and M, all others were acquired directly in the experiment; The η as in Table 1 above, calculated by Formula (13); The M was calculated by substituting the experimentally acquired data into formula (14).

Following correct operation, the M and η relationship formula (1) yields the formula (14).

$$M = \sqrt{\frac{\eta R_1 (R_2 + R_L)^2}{\omega_d^2 R_L - \omega_d^2 \eta (R_2 + R_L)}} \tag{14}$$

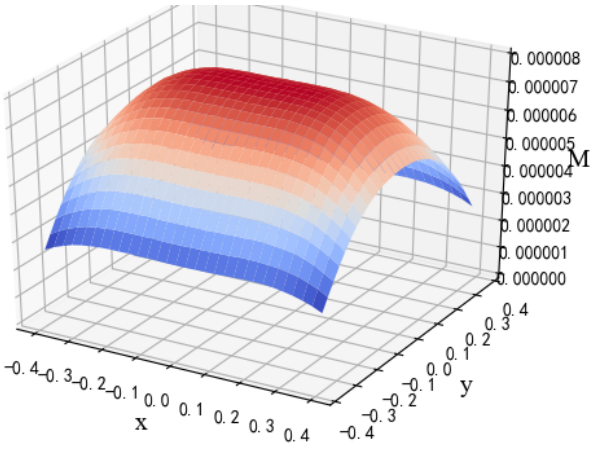

Fig. 15: M distribution map.

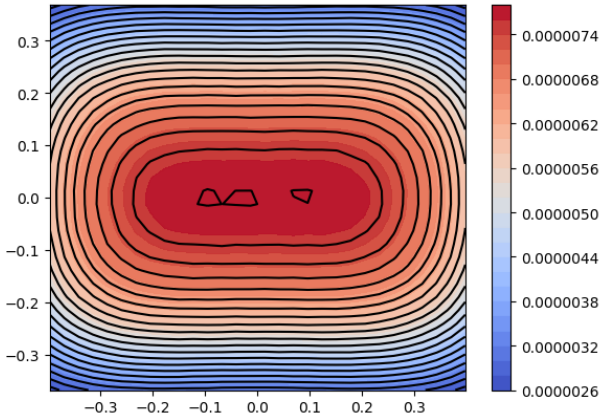

Fig. 16: M distribution contour map.

Where, M, RL, R1, R2, ω_d, η, are the same as the definition above.

The four figures Fig. 15 Fig. 18 are all drawn by the experimental data Table 2 with the help of computer software. It is not difficult to see that these four figures are very close to the above theoretical analysis figures Fig.5 Fig. 8.

Looking up Table 2, the maximum value of the M is as follows:

$$\text{Mmax} = 7.76 \times 10^{-6}(H) \tag{15}$$

The maximum value of the M just matches the maximum value 80.38% of η. The maximum value of M is equal to the highest value Mmax = 7.76×10^{-6} (H) determined by the above theoretical analysis with the error value 0.11×10^{-6} (H). The reason for the error may be that the design structure of L1 and the L2 is not perfect, or the magnetic field shielding is not well done; However, the error ratio is roughly 1.4%, which is not significant and does not affect the research of this subject. Looking up the experimental data, the maximum value of M, there are several positions corresponding to

Tab. 1: Experiment 1: MCR-WPT experiment (D=20CM, Ui=400V, RL=70Ω).

Drive frequency f, KHz	Input voltage Ui, V	Input current Ii, A	Output voltage Uo, V	Output current Io, A	WPT efficiency η,%
80.0	400	6.59	367.3	5.2	73.10
81.0	400	6.75	373.1	5.3	73.64
82.0	400	6.86	380.3	5.4	75.27
83.0	400	7.06	390.1	5.6	76.95
84.0	400	7.17	397.2	5.7	78.58
85.0	400	7.61	411.7	5.9	79.56
85.1	400	7.59	411.7	5.9	79.80
85.2	400	7.61	413.1	5.9	80.11
85.3	400	7.93	422.5	6.0	80.41
85.4	400	7.55	412.0	5.9	80.24
85.5	400	7.57	411.5	5.9	79.89
85.6	400	7.48	407.9	5.8	79.47
86.0	400	7.34	401.9	5.7	78.66
87.0	400	7.13	392.6	5.6	77.22
88.0	400	6.99	384.1	5.5	75.33
89.0	400	6.88	376.8	5.4	73.70

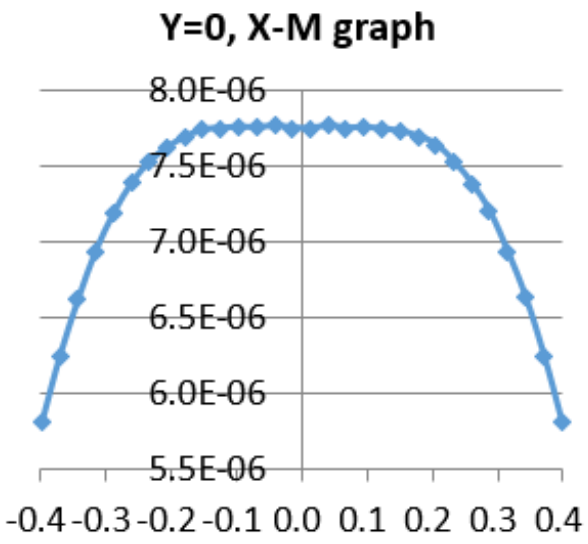

Fig. 17: Y=0,X-M graph.

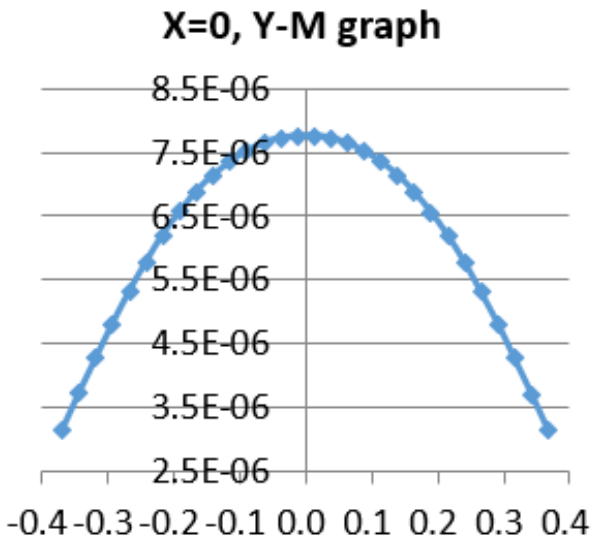

Fig. 18: X=0, Y-M graph.

Tab. 2: Experiment 2: Mutual induction distribution experiment (D=20CM,Ui=400V f=85.3KHz, RL=70Ω)

X coordinate m	Y coordinate m	Input voltage Ui, V	Input current Ii, A	Output Voltage Uo, V	Output Current Io, A	WPT Efficiency η, %	Mutual Inductance M,H
-0.397	-0.368	400	7.94	267.97	3.83	32.30	2.64E-06
-0.370	-0.368	400	7.95	278.59	3.98	34.87	2.80E-06
-0.342	-0.368	400	7.94	287.22	4.10	37.09	2.94E-06
-0.315	-0.368	400	7.94	292.55	4.18	38.52	3.03E-06
-0.287	-0.368	400	7.94	296.67	4.24	39.59	3.10E-06
-0.260	-0.368	400	7.95	299.47	4.28	40.30	3.14E-06
-0.233	-0.368	400	7.93	300.47	4.29	40.66	3.17E-06
-0.205	-0.368	400	7.94	302.13	4.32	41.06	3.19E-06
.....Part of the data is omitted, and the following is the data around the maximum value of M							
-0.096	-0.013	400	7.94	422.71	6.04	80.33	7.74E-06
-0.068	-0.013	400	7.94	422.69	6.04	80.38	7.75E-06
-0.041	-0.013	400	7.93	422.41	6.03	80.33	7.74E-06
-0.014	-0.013	400	7.94	422.72	6.04	80.38	7.76E-06
0.014	-0.013	400	7.94	422.69	6.04	80.36	7.75E-06
0.041	-0.013	400	7.94	422.65	6.04	80.35	7.75E-06
0.068	-0.013	400	7.93	422.40	6.03	80.32	7.74E-06
0.096	-0.013	400	7.93	422.44	6.03	80.36	7.75E-06
0.123	-0.013	400	7.93	422.39	6.03	80.33	7.74E-06
0.151	-0.013	400	7.94	422.61	6.04	80.29	7.73E-06
0.178	-0.013	400	7.94	421.91	6.03	80.07	7.68E-06
0.205	-0.013	400	7.94	421.34	6.02	79.82	7.62E-06
.....900 lines of data in total							

the maximum value: (-0.096,-0.0127), (-0.0960,0.0127), (-0.041,0.0127), (0.096,0.0127). These positions are all near the coordinate origin; By observing Fig. 15 and Fig. 16, we can also estimate that the maximum value is near the coordinate origin.

As a result, the experimental data supports the theoretical explanation of the M distribution presented in this study.

7. Conclusions

Theoretical analysis and experimental evidence presented above demonstrate that the greatest M, between L1 and L2, is situated close to the L1 center point, which serves as the coordinate origin. When the horizontal displacement of the two coils exceeds the range of X∈[-0.1, +0.1], Y∈[-0.01, +0.01], the M drops rapidly. The greatest value of M is still attained when the displacement of the two coils is within 0.1m along the x-axis or within 0.01m along the y-axis. As a result, it is essential to make sure that the M is maximized to achieve efficient wireless power transmission across the MCR-WPT system. This work investigated the spatial distribution of the M, providing a theoretical foundation for the design of the location in a MCR-WPT system.

Acknowledgment

This work is funded by the 2022 Guangxi university scientific research project, China. The project name is: "Research on Automatic Positioning System for Wireless Charging of Automobile Based on Maritime Search and Rescue Algorithm" (No. 2022KY1335).

Author Contributions

Junlong Zheng: Conceptualization, Data curation, Programming, Writing -original draft, Writing-editing. Chaiyan Jettanasen: Overall guidance, reviews, suggestions for modifications.

References

[1] Liu Tao, *Circuit Research of Magnetically Coupled Resonance Wireless Charging System for Electric Vehicle[D]*, Southwest University of Science and Technology.

[2] Lionel Pichon. Electromagnetic analysis and simulation aspects of wireless power transfer in the domain of inductive power transmission technol-

ogy[J]. *Journal of Electromagnetic Waves and Applications*, 2020, vol. 34, no. 13, 1719–175 DOI: 10.1080/09205071.2020.1799870.

[3] Rui Feng, Nina Roscoe, et al. Magnetic Field Distribution in a WPT System for Electric Vehicle Charging[J]. *Progress In Electromagnetic Research Symposium (PIERS)*, Shanghai, China, 8–11 August 2016, DOI: 10.1109/PIERS.2016.7735864

[4] Yang Yang, Jinlong Cui, et al. Design and Analysis of Magnetic Coils for Optimizing the Coupling Coefficient in an Electric Vehicle Wireless Power Transfer System[J]. *Energies*. 2020, 13, 4143. DOI: 10.3390/en13164143.

[5] Kafeel Ahmed Kalwar, Saad Mekhilef, et al. Coil Design for High Misalignment Tolerant Inductive Power Transfer System for EV Charging[J]. *Energies*. 2016, 9, 937; DOI: 10.3390/en9110937.

[6] Sangwook Park. Evaluation of Electromagnetic Exposure During 85 kHz Wireless Power Transfer for Electric Vehicles[J]. *IEEE Transactions On Magnetics*, vol. 54, No. 1, January 2018. DOI: 10.1109/tmag.2017.2748498.

[7] Haris Gulzar, Noor ul Ain, Talha Zahid, et al. A Comprehensive Electromagnetic Design, Simulation and Analysis of Wireless Charging Coils for Large Power Applications[C]. *2018 Progress In Electromagnetics Research Symposium (PIERS - Toyama)*, Japan, 1–4 August. DOI: 10.23919/PIERS.2018.8598241.

[8] Rupesh Kumar Jha, et al, Performance Comparison of the One-Element Resonant EV Wireless Battery Chargers. *IEEE Transactions On Industry Applications*, Vol.54 No.4 May/June 2018. DOI: 10.1109/TIA.2018.2796058.

[9] Ihssen Jabri, Adel Bouallegue, Fethi Ghodbane, Misalignment controller in wireless battery charger for electric vehicle based on MPPT method and metaheuristic algorithm, *Wireless Netw* (2018) 24:2375–2396, DOI: 10.1007/s11276-017-1474-5.

[10] Yang Defu, Song Bei, Wang Yuqing, *Analysis of problems in measuring air permeability[J]*, Journal of Yanan University, Sept.2005. DOI: 10.3969/j.issn.1004-602X.2005.03.017.

[11] L Zhai, G Zhong, et al, Research on Magnetic Field Distribution and Characteristics of a 3.7 kW Wireless Charging System for Electric Vehicles under Offset[J], *Energies*, 2019, vol. 12, issue 3, 1-21, DOI: 10.3390/en12030392.

[12] Yang Yunhu, Chen Shuai, On the Influence of Key Variables on System Efficiency inWireless Charging System for Electric Vehicles[J], Journal of Changzhou Institute of Technology, Oct. 2020. DOI: 10.3969/j.issn.1671-0436.2020.05.004.

[13] Kuang Xiangjun, Calculation of space magnetic field for any quadrilateral current-carrying coil[J]; *College Physics*; Vol.36, No.4, Apr. 2017. DOI: 10.16854/j.cnki.1000-0712.2017.04.007.

[14] Tan Juhua, Li Xiaofang, Guo Xiaochun, Design and Optimization Analysis of Wireless Charging Coil for Magnetically Coupled Resonance Electric Vehicle[D], *Journal of Shenyang University of Technology*, Jan. 2020.

[15] I.S. Grant, W.R. Phillips, *Manchester Physics*, John Wiley & Sons, Electromagnetism (2nd Edition)[M], 2008, ISBN 978-0-471-92712-9.

[16] Miller J M, Jones P T, Li J M, et al. ORNL Experience and Challenges Facing Dynamic Wireless Power Charging of EV's[J]. *IEEE Circuits & Systems Magazine*, 2015, 15(2):40-53. DOI: 10.1109/MCAS.2015.2419012.

[17] Chen Chen, Huang Xueliang, Tan Linlin, et al. Electromagnetic Environment and Security Evaluation for Wireless Charging of Electric Vehicles, *Transactions of China Electrotechnical Society*, Oct. 2015 Vol. 30 No. 19, DOI: 10.19595/j.cnki.1000-6753.tces.2015.19.010.

About Authors

Junlong ZHENG is currently a Ph.D. Research Fellow in King Mongkut's Institute of Technology Ladkrabang, Thailand. At the same time, he is a senior engineer, engaged in teaching and scientific research in Guangxi Electrical Polytechnic Institute, China. His research interests include Electrical Engineering and New Energy Vehicle Technology.

Chaiyan JETTANASEN (corresponding author) is currently engaged in teaching and scientific research in King Mongkut's Institute of Technology Ladkrabang, Bangkok, Thailand, and his main research direction is electrical engineering